LEVEL II

①

⑥

Effective Source Functions From Local

Surface Measurements

Woodward-Clyde Consultants   New

380 W. Del Mar, Pasadena, CA 91105

⑨ Mid Term Technical Report. 15 Apr-15 Jul 81 ⑨

For Period April 15, 1981 to July 15, 1981

⑩ David M. Cole

Sponsored By

Defense Advanced Research Projects Agency (DOD)

ARPA Order No. 4223

⑮   new

Under Contract No. MDA903-81-C-0269 issued by

√√ ARPA Order-4223

Department of Army, Defense Supply Service-Washington,

Washington, D.C.   20310

DTIC
S ELECTE D
SEP 4 1981

New   412520   D

81 9 02 095

⑪ 31 July 31, 1981

⑫ 32   i

ARPA Order No. 4223

Contract No. MDA903-81-C-0269

Effective Date of Contract: April 15, 1981

Contract Expiration Date: October 15, 1981

Contractor: Woodward-Clyde Consultants

        380 W. Del Mar Boulevard

        Pasadena, CA   91105

Principal Investigator: David M. Cole

Phone Number: (213)792-1159

DTIC
ELECTE
S SEP 4 1981
D

D

ii

Technical Summary

The objective of the work presented here is to develop and evaluate
the adequacy of an elastic source description of the near-in surface record-
ings of ground motion from the underground nuclear test "Milrow".
Generalized ray, mode and discrete wavenumber techniques have been applied
to model four of the available vertical and radial L-7 records. Prelimin-
ary results indicate that an elastic description will be adequate for
distances greater than 7 km. The preferred RDP at this point is a
Helmberger-Hadley source with B = 2, K = 5 sec^{-1} and Ψ_{∞} = 1 x 10^{11} cm^3.
Comparison of the predicted teleseisms using this source with the
teleseismic data yields an average t* of 1.0 sec. No clear azimuthal
trends are manifest in the teleseismic data. No evidence of nonlinear
or anelastic behavior has been detected for data in the range 7. to 11.5 km.
In the future, a refined crustal structure for the test site will be
developed, and a definitive source function for both Cannikin and Milrow
will be obtained.

A Preliminary Milrow Source Function

The objective of this study is to determine a source time function appropriate for the nuclear explosions "Milrow" and "Cannikin". The reason for this is two-fold: 1) to confirm linearity in the epidistance region of 7 to 20 km, and 2) to determine the source strength so that a far-field determination of t* is possible.

Vertical and radial velocity from four sites with ranges of 7, 8, 9.8 and 11.5 km comprise the data set used here for Milrow (figures 1 and 2). The first 1 to 1 1/2 seconds of the wave train at a given site are interpreted in terms of bodywaves and are modeled with generalized rays. This response is added to the fundamental mode Rayleigh wave synthetics to construct a complete seismogram (figure 3).

For the modeling procedure only the two primary rays are used; P and pP (for the layered structures used this usually amounted to 12 to 16 actual ray descriptions). The fit of the seismogram to observations is controlled by two things; the earth structure and the source time function. These structures were available: 1) Engdahl's (1972) synthesis of well-log data and arrival times, 2) Burdick and Helmberger's (1979) modification of Engdahl's model and 3) the drill logs. Each of these models was tested and only 2) was rejected on the basis of being too slow. The final model has a top (the upper 3 km) determined from a combination of the Milrow and Cannikin drill data and the bottom of Engdahl's model (see table). For any reasonable time function, the structure has a strong effect on the relative amplitude of the first up and downswings. The ratio of the radial to vertical amplitude is a function of the SV to P ratio. The model was adjusted to give the best agreement for the four stations, which gives P/SV=1.6 in the top layer.

2

The time function which was used is described by Helmberger and
Hadley (1981) (figure 4). The fit of the time function is determined
by the pulse width and the overshoot. The stations at close range
give the simplest pulse (i.e., structure, such as triplications, are
not important), so the stations at 7 and 8 km were used to determine
K and B. It was decided that ψ with K=5 sec^{-1} and B=2 gives the best
fit. This also allows a direct comparison of Milrow with Jorum and
Handley. The source strength, or Ψ_∞, was determined by averaging
the ratio of the observations to synthetic for the four stations.
This gives ψ_∞(5, 2) =1.2 x 10^{11} cm^3; see figure 5. Note that this
systematically overestimates the surface waves for increasing ranges
(figure 3). A slightly smaller value of ψ_∞ (5, 2)=1 x 10^{11} cm^3 was
chosen as a compromise.

The Rayleigh wave portion of the composite synthetics of figure 3 is
composed of only the fundamental Rayleigh wave mode. The upper P wave velo-
city and density structure for the Rayleigh wave model is from the Cannikin
detonation point model given in Murphy and Bennet (1979). The P velocity
structure below 9 km is from Engdahl (1972). The shear wave structure
below 3.3 km was taken from S wave phase studies in Alaska (Noponen and
Burnett, 1979). Above 3.3 km the S wave velocities were obtained from
an assumed Poisson ratio of 0.25 (see table).

The instrument response for the L-7 velocity seismograph system
was obtained from a minimum phase calculation using the velocity
sensitivity amplitude versus frequency response given in Navarro
and Wuollet (1972). The instrument system essentially performs a
band limited derivative of the ground motion and yields a filtered
velocity seismogram. This instrument was used in all the synthetic
seismograms for this report.

3

In order to evaluate the effectiveness of describing the latter portion of the near-field ground motion using only the fundamental Rayleigh wave mode, we calculated a complete radial seismogram at ranges of 7 and 11.5 km using the Discrete Wavenumber Finite Element (DWFE) Program developed by Olson (1978).

The DWFE seismograms with superimposed fundamental mode Rayleigh wave seismograms are shown in figure 6. The time and amplitude scales are the same for all four synthetics. The initial times for the two techniques are shifted so as to obtain the best fit and the amount of shift is indicated at the left of each superposition. The amplitude agreement is very good and the maximum peak to trough amplitude agreement is excellent. The difference is on the order of 1%. The difference in absolute time is on the order of .2 to .3 sec.

In the comparison of observed with theoretical DWFE radial seismograms in figure 7 we see that our model structure results in a synthetic of duration less than the observed; i.e. the time separation between the P wave and Rayleigh wave phases is too small. This inadequacy could be due to an over estimation of the shear wave velocity near the surface. A lower Poisson ratio for near surface rock is more physical and would result in lower shear velocities.

Another indication of lower shear velocity near the surface is the presence of the long period phase in between the P wave and Rayleigh

4

wave on the observed radial seismograms and its absence on the verticals
(see figure 2). We interpret this phase as a P_L wave composed of SV
energy arriving at a steep angle of incidence. This type of motion
requires a structure with low Poisson ratios near the surface.

Another discrepancy between the observed and theoretical radial
seismograms seen in figure 7 is the relative excitation between the P
and Rayleigh wave phases. The ratio of theoretical P to Rayleigh
amplitudes is small compared to the observed. This is also true for
the theoretical composite seismograms, both radial and vertical, in
figure 3 when compared to the observed seismograms in figure 2 at all
four stations.

In figure 6 we had compared the Rayleigh wave mode synthetic with
the DWFE calculation and found the agreement very good for the Rayleigh
wave portion of the synthetics. On the other hand, if we compare the
P wave portion of the DWFE with the generalized ray P wave of the
composite synthetics in figure 3, we find that the DWFE P wave is
smaller by approximately 25%. This discrepancy is due to the practical
frequency limitation of the DWFE calculation. Since the cost of a DWFE
calculation is proportional to the frequency cubed, we restricted our
calculation to frequencies less than 5 hertz. The 10 hertz needed to
realistically model the P wave as seen through the L-7 seismometer
(figures 2 and 3) is too expensive for DWFE calculations on a routine
basis.

Since one of our prime tasks is to analyze these near-field surface ground motions and estimate the detailed character of the seismic source function, we investigated the possibility of whether a reasonable seismic source can be found to bring the theoretical ratio into agreement with the observed. The frequency content of the P-wave and Rayleigh wave differ slightly, but realistic variations for megaton class events at these relatively short frequencies might be difficult to obtain.

As a starting point in this analysis, we look at the step explosion RDP or moment response obtained in the DWFE calculation. This is the Green's function which would be used in a systematic inversion procedure and is shown in figure 8. The P-wave and P_L wave are actually larger than the Rayleigh wave, thus by making our source function more steplike we can increase the theoretical P to Rayleigh ratio.

As noted before the source function used in the previous synthetics is the Helmberger-Hadley RDP shown in Figure 4. By increasing K, we increase the source rise time and by reducing B we decrease the source overshoot, both variations tending to make the source more steplike. In figure 9 we show synthetics for a $K=8$ sec^{-1} which is an increase over the $K=5$ sec^{-1} value used in figure 7. As predicted, the theoretical P to Rayleigh ratio is increased compared to earlier values. This effect will be exploited to obtain a better source function in the future.

Determination of t* from Milrow Data

Given the source time function and source region velocity structure determined from the near field modeling it is possible to place constraints on a global average of t* by propogating the near field results to teleseismic distances. Both Milrow and Cannikin produced an extensive long period P wave data set as well. Figure 10 shows the short period wave forms for Milrow recorded on WWSSN instruments. The azimuthal coverage for stations with $\Delta < 95°$ is relatively good, better than for NTS. All of the data shown is in the range $30° < \Delta < 95°$ except for TRN at $\Delta = 99°$. There are very few usable long period P waves for Milrow. Several features are notable in this data set:

1) The higher frequency stations in Europe show a shoulder in the 2nd upswing that may be pP; see STU, MAL, COP at .8 to 1.0 sec. back. It is possible that t* to these stations is low enough to show this interference.

2) AAM, WES, and SHA show a strong interference in the 2nd upswing which commences about 1.5 - 1.8 sec. back. The resulting waveforms are very similar to the Cannikin recordings in the U. S. This phase is much too late for the expected pP.

3) As is usually found, the waveforms are most coherent over the first 1 1/2 cycles, with receiver structure dominating later portions of the waveform.

Amplitudes for Milrow

The AB and BC amplitudes (see figure 11) for the data shown in figure 10 were measured as well as for 5 additional stations which are

7

not digitizable. They were corrected for instrument gain to millimicrons of ground displacement and then corrected for geometric spreading to a standard distance of 30° using the curve for $\frac{1}{R}$ in Langstan and Helmberger (1976). The average AB amplitude is 1046 mμ (N = 44) and the average BC amplitude is 1615 mμ (N = 43). If we use a reference distance of 50°, the averages are AB: 792 mμ and BC: 1224 mμ. If one corrects the Handley and Jorum events analyzed by Hadley and Helmberger (1981) one obtains BC amlitudes for Jorum: 1024 mμ at 30° and 776 mμ at 50°. For Handley one obtains 1431 mμ at 30° and 1084 mμ at 50°.

Thus, Milrow is slightly larger than Handley. In figure 11 the amplitudes from Milrow (corrected to 30°) are shown plotted as a function azimuth. Here we are testing for the type of azimuthal trend seen in the NTS data (compare to Figure 9 of Hadley and Helmberger (1981)). The U. S. stations (azimuths 35° - 80°) tend to have higher amplitudes than the European stations (azimuthus 330° - 20°) but overall there is not a clear pattern, such as might be introduced by the Aleutian slab, etc. This data is much denser than for the NTS events and it looks as though there is no obvious azimuthal amplitude trend biasing the averages.

Given the reliable teleseismic amplitudes we can use the near field solution to predict the teleseismic amplitudes. The source structure used in synthesizing the teleseisms was that determined in the preliminary analysis of the near field Milrow data. This structure merges smoothly with a JB mantle structure. The synthetic step response for a distance

8

of 50° was computed using the Cagniard-de Hoop procedure. A finely layered structure (layer thickness is ~ 5 km in the vicinity of the turning ray) with 150 total layers was employed. The range 50° was chosen to have the rays bottom in a smooth part of the mantle. Only primary reflections are included in generating the responses. For the Ψ_∞ determined above ($\Psi_\infty = 1.0 \times 10^{11}$ cm^3) the BC amplitudes of the synthetic with K = 5 sec^{-1}, B = 2 and t* = 1.0 sec. is BC = 1209 mμ. This number is based on a more typical receiver function compared with the receiver function for the Milrow source region, which has low values for $\alpha = 3.0$, $\beta = 1.7$. This amplitude is very close to the BC amplitude of 1224.

The synthetic at 50° is compared with the data from GDH, ALQ and HKE in figure 12.

RVP for a Laboratory Experiment

Radial velocity measurements from a chemical explosive detonated in a small (1/3 meter) block of Dolomite were processed to obtain reduced velocity potentials. The data were taken from Larson (1981) for the radii 7.64, 10.25 and 14.08 cm. If the deformations produced in this experiment were ideally elastic and linear for all distances at which the measurements were obtained, the radial velocity would be described by a reduced velocity potential $\dot{\psi}(t)$ where

$$V(R,t) = \frac{-\partial}{\partial R} \frac{1}{R} \dot{\psi}(t-R/\beta)$$

and $V(R,t)$ is the measured radial velocity at distance R from the center of symmetry. Solving for $\psi(t)$ one obtains

$$\dot{\psi}(t) = \alpha R \int_{-\infty}^{t} e^{\alpha(p-t)/R} V(R, p + R/\beta) \, dp$$

For the ideal case $\dot{\psi}(t)$ computed in this manner will not depend on the measurement radius R, provided that the correct value of the compressional velocity is used and the experimental material is homogeneous. Larson's data are reproduced in Figure 13. The peak velocity there decays as $R^{-1.7}$. Propagation velocities obtained from timing the first arrivals range from 6.87 to 6.71 km/sec. The velocity used in the processing here was 6.85 km/sec. It should be noted that the velocity traces were truncated in the original data at the first zero crossing and should have continued on through negative velocity values. The RVP

10

for each data time series is shown in Figure 14, truncated at the point where data ceased. Also shown in Figure 14 are the near and far field portions of the velocity reconstructed from the RVP, confirming that the signal is dominated by the far field term. The complete velocities reconstructed from the RVP's are shown in Figure 15 for the different data radii. Reconstruction of the velocity at a radius other than that at which it was measured is nearly a scalar multiplication because of the far field dominance. The notable feature of the reconstructions is that the peak velocity is decaying much more rapidly than R^{-1}, but the tail of the wave is decaying at about the R^{-1} rate for elastic behavior. Note also that the initial peak broadens with distance. It might thus be possible to obtain an approximate mathematical model of the anelastic attenuation here which represents the attenuation of the peak using a linear filter similar to other Q filters by reducing high frequency amplitudes. The effect of the filter on the RVP's would be relatively minor, since they are composed of lower frequencies. The relevance of such a filter to earth phenomena would, of course, depend on the actual physical mechanisms involved in the attenuation process. The difference in time scales between the laboratory experiments and the underground tests is large; 10^{-5} sec for the laboratory as compared to 10^{-1} sec for the field tests. The peak volumetric strain in the lab experiment here is about 10^{-2} and the peak strain at several kilometers from Cannikin was on the order of 10^{-3} or more. The peak strain rate in the lab experiment was 10^3 sec^{-1} and the peak strain rate from Cannikin was about 10^{-2} sec^{-1}.

Conclusions

Even with a preliminary near field velocity structure, we have shown qualitatively that near field surface ground motions can be used to estimate the seismic character of an explosion source. We have also demonstrated that a composite seismogram composed of the generalized ray P-wave and the fundamental mode Rayleigh wave can be inexpensively used for routine reconnaissance, providing information on both source region structure and source character. We intend to improve our elastic structure for Milrow and Cannikin and obtain realistic source functions for both events.

The DWFE seismogram is especially helpful in applying constraints to the velocity structure. Because of frequency bounds it may not be feasible for the high frequency resolution of the source function using inversion techniques.

Our next step is to improve the P-wave portion of the instrument filtered Green's function by replacing it with the instrument filtered step response of the generalized-ray P phase. These new composites will be used in a formal inversion of the Milrow and Cannikin ground-motion for best estimates of their respective source functions.

The short period teleseismic waves for Milrow show some variability in waveform and appreciable amplitude scatter, but lack a distinct azimuthal amplitude pattern. The average teleseismic amplitude is matched using a value of t* of 1.0.

A laboratory experiment on dolomite has been reviewed and it appears that the peak motions are in the far field and decay anelastically. It may be possible to model the peak decay effects and extend the mathematical representation to model near source anelastic effects in the Earth, provided that the physical mechanism of anelastic attenuation is sufficiently similar. This is an open question because of some large differences in the time scales and strain rates in the lab experiments compared to the field experiments.

References

Burdick, L. and D. Helmberger (1979) Time functions appropriate for
nuclear explosions, Bull. Seism. Soc. Am., 69, 957-974.

Engdahl, E. R. (1972). Seismic effects of the Milrow and Cannikin
nuclear explosions. Bull. Seism. Soc. Am., 62, 1411-1423.

Helmberger, D. V. and D. M. Hadley (1981) Seismic source functions
and attenuation from local and teleseismic observations of the
NFS events Jorum and Handley, Bull. Seism. Soc. Amer., 71, 51-67.

Larson, D. B. (1981). Explosive energy coupling in geologic
materials. Preprint UCRL-85662. Lawrence Livermore Laboratory.

Murphy, J. R. and T. J. Bennet (1979). A review of available free-
field seismic data from underground nuclear explosions in alluvium,
tuff, dolomite, sandstone-shale and interbedded lava flows.
Systems, Science and Software, Topical Report, SSS-R-80-4216, 1-143.

Navarro R. and G. M. Wuollet (1972). The L-7 velocity seismograph
shaking-table results. NOAA Technical Report, ERL-254-ESL-26, 1-48.

Noponen, I. and J. Burnett (1979) Alaskan regional data analysis.
Teledyne Geotech Technical Report, AL-80-1, Vo. II, 1-142.

Olson, A. (1978). Synthesizing ground motion using a discrete
wavenumber/finite element representation. EOS, Trans. Am. Geophys.
Union, 59, P. 1128 abs.

TABLE OF ELASTIC LAYER MODELS

GENERALIZED RAY MODEL

P Velocity (km/sec)	S Velocity (km/sec)	Density (gm/cc)	Depth to Top of Layer (km)	Layer Thickness (km)
3.0	1.7	2.30	0.00	0.35
3.7	2.1	2.40	0.35	0.55
4.2	2.4	2.40	0.90	0.60
4.7	2.7	2.40	1.50	0.35
5.1	2.9	2.5	1.85	0.10
5.5	3.17	2.6	1.95	6.65
6.9	3.98	2.81	8.60	28.0
8.2	4.7	3.2	36.6	

FUNDAMENTAL RAYLEIGH MODE

P Velocity (km/sec)	S Velocity (km/sec)	Density (gm/cc)	Depth to Top of Layer (km)	Layer Thickness (km)
3.0	1.7	2.3	0.00	0.35
3.7	2.1	2.4	0.35	0.55
4.2	2.4	2.4	0.90	0.65
4.7	2.7	2.4	1.55	0.30
5.5	3.1	2.6	1.85	1.45
5.9	3.5	2.7	3.30	5.7
7.0	4.00	2.9	9.00	28.0
8.2	4.7	3.2	37.00	

DWFE

P Velocity (km/sec)	S Velocity (km/sec)	Density (gm/cc)	Depth to Top of Layer (km)	Layer Thickness (km)
3.0	1.7	2.3	0.00	0.20
3.7	2.1	2.4	0.20	0.65
4.2	2.4	2.4	0.85	0.48
4.7	2.7	2.4	1.33	0.50
5.1	2.9	2.5	1.83	0.10
5.5	3.17	2.6	1.93	6.65
6.9	3.98	2.81	8.58	* 20.0

* Bottom layer is terminated by a rigid bottom at a depth of 28.58 km.
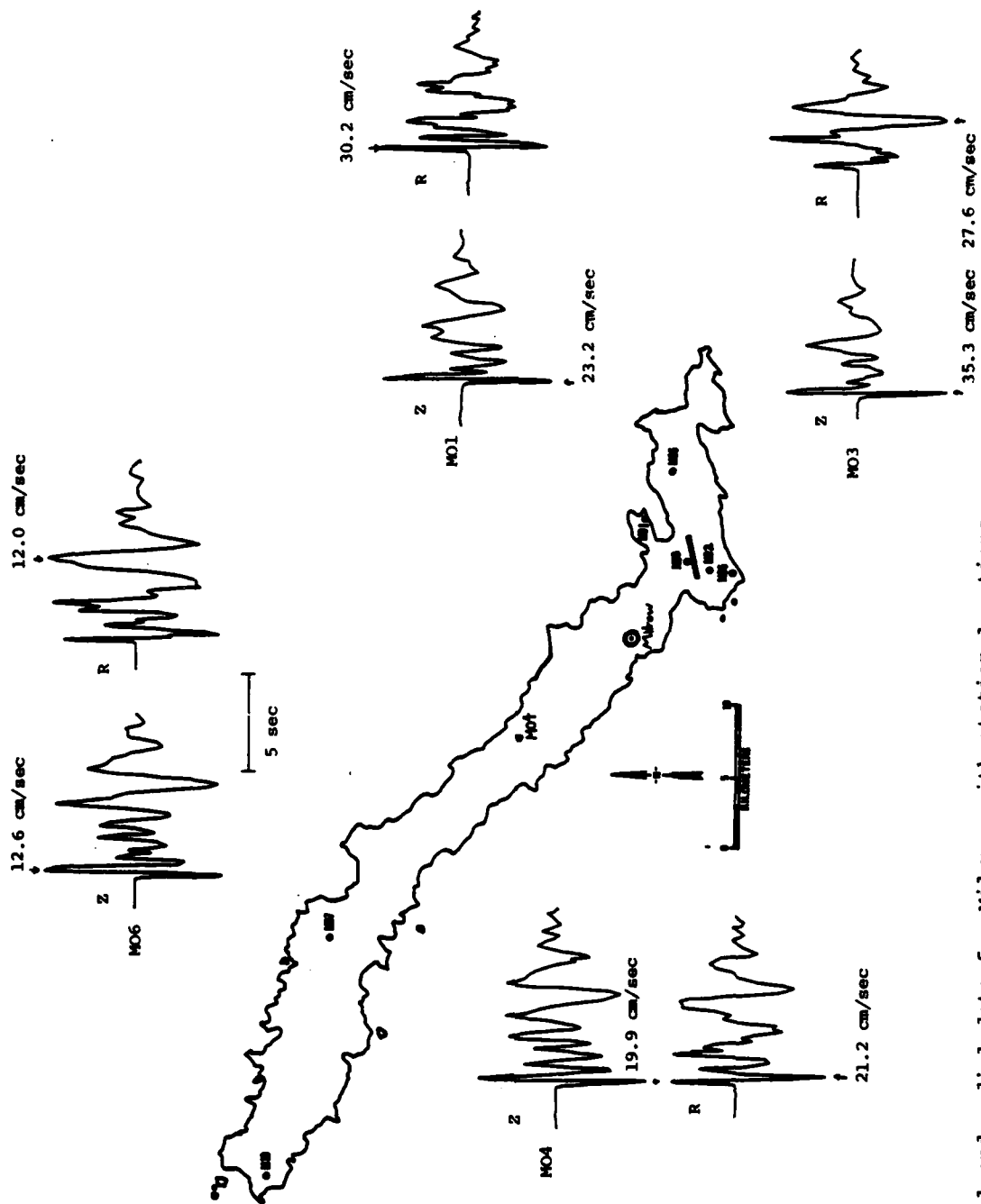
Figure 1. Vertical and radial data for Milrow, with station locations. Epicentral distances are, for stations 3, 1, 4, 6; 7 km, 8 km, 9.8 km, 11.5 km.

16
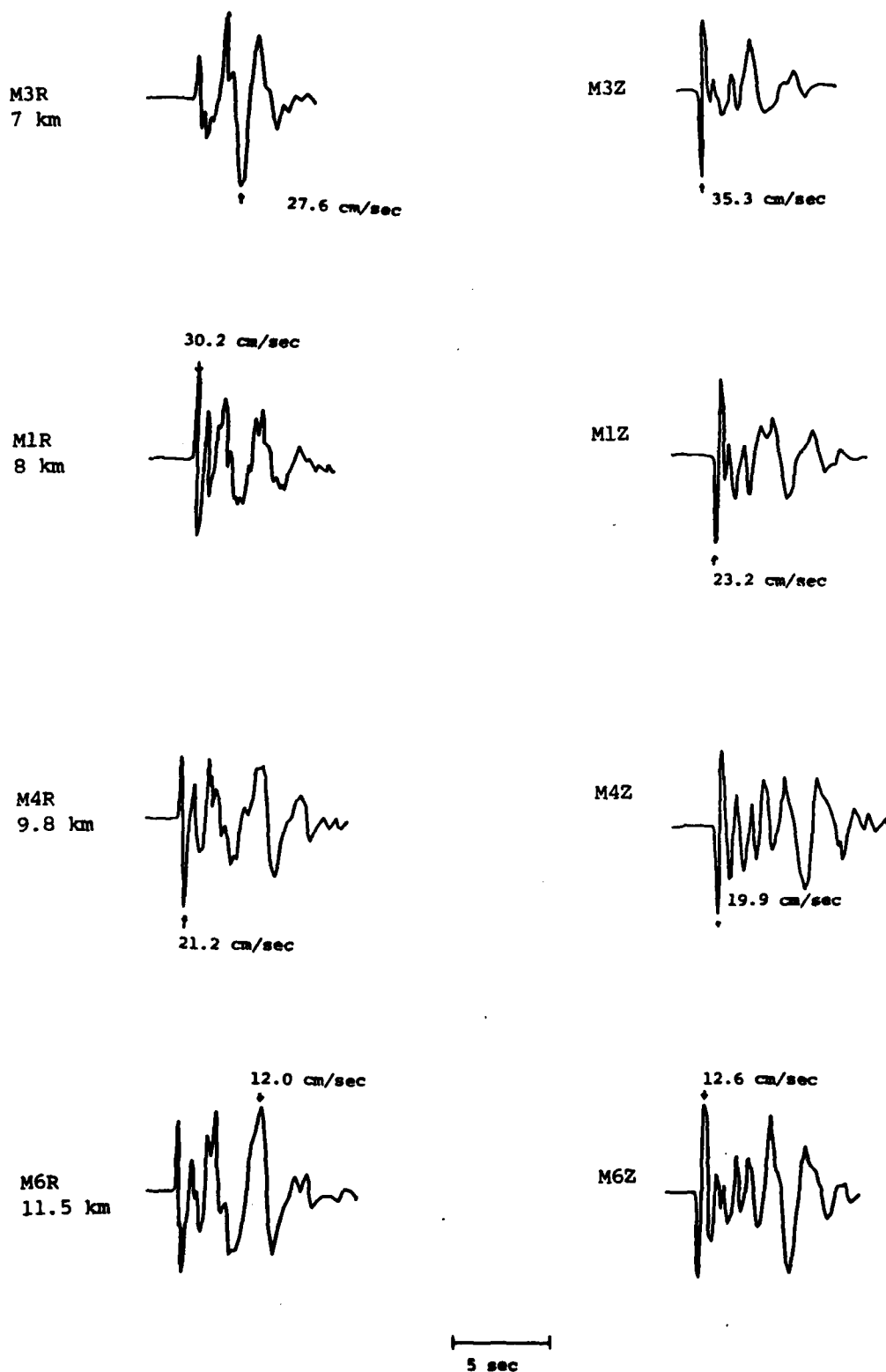
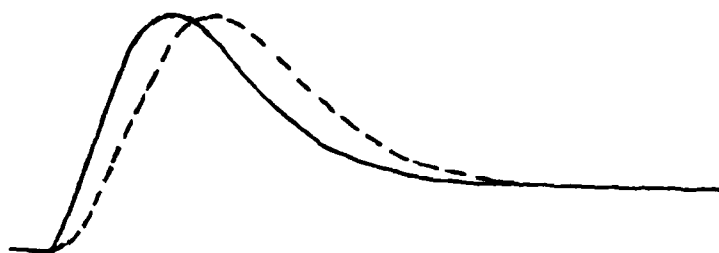Figure 2. Radial and vertical data for Milrow, stations 3, 1, 4, 6.
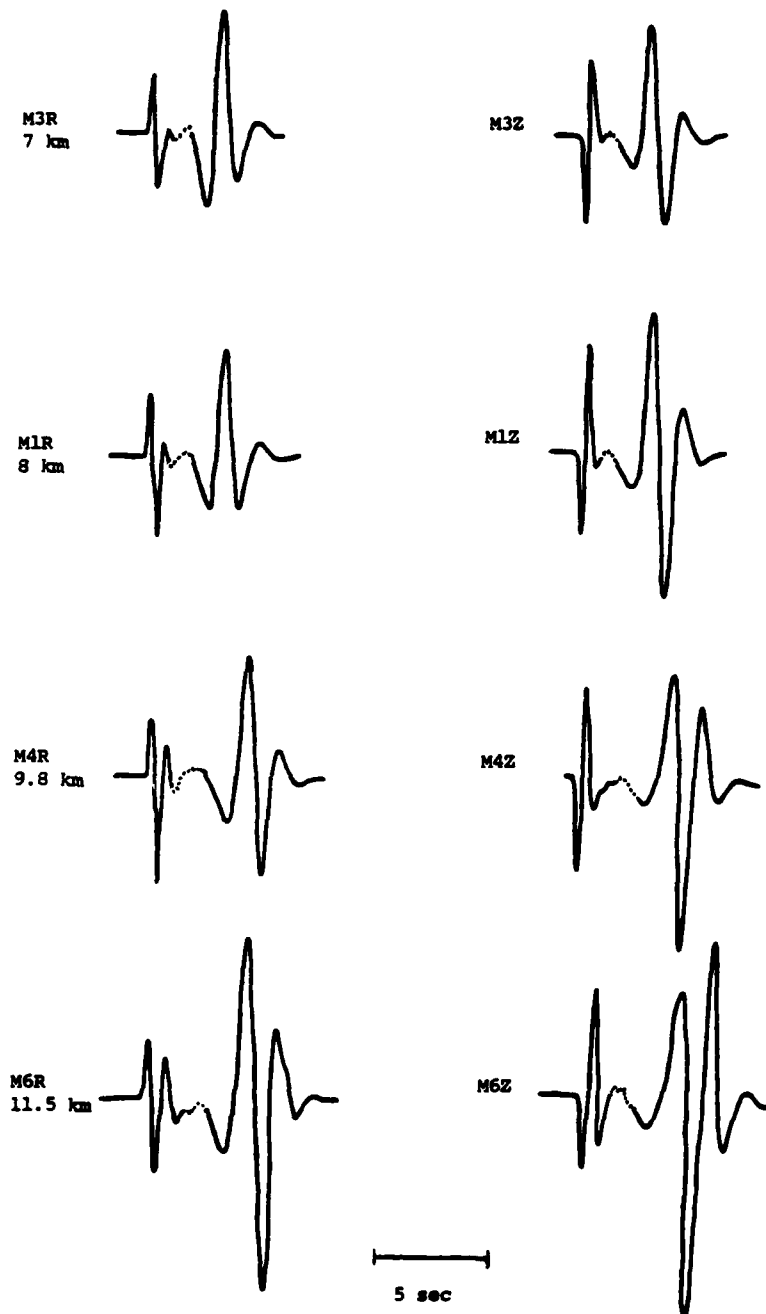
Figure 3. Synthetics for Milrow stations 3, 1, 4 and 6. First part of each trace is from Generalized Ray calculation; the latter is the fundamental Rayleigh mode.

Haskell RDP: $B = 0.6$, $k = 5.$ sec^{-1}

Helmberger-Hadley: $B = 2.$, $K = 5.$ sec^{-1}

Figure 4. Source time functions.

23.2 cm/sec

	M01	Vertical observation
	ψ (5,3)	$\psi_\infty = .83 \times 10^{11}$ cm^3
	ψ (7,2)	$\psi_\infty = .73 \times 10^{11}$ cm^3
	ψ (5,2)	$\psi_\infty = 1.20 \times 10^{11}$ cm^3
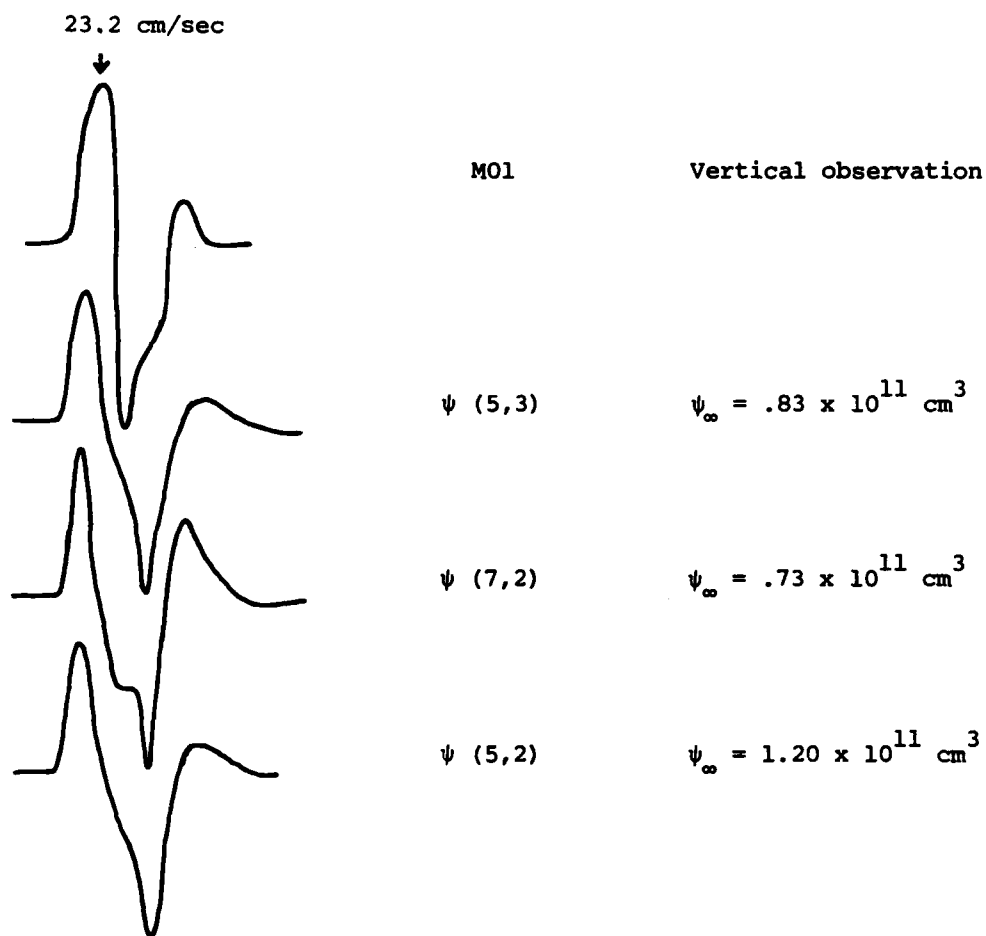
Figure 5. Vertical observation at M01 and synthetics for different values of (K,B) and ψ_∞. Range is 8. km.

Fundamental Rayleigh mode ------

DWFE ———

Range   7. km

Range   11.5 km

$$\psi_\infty = 10^5 \, m^3$$
$$K = 5. \, sec^{-1}$$
$$B = 2.$$
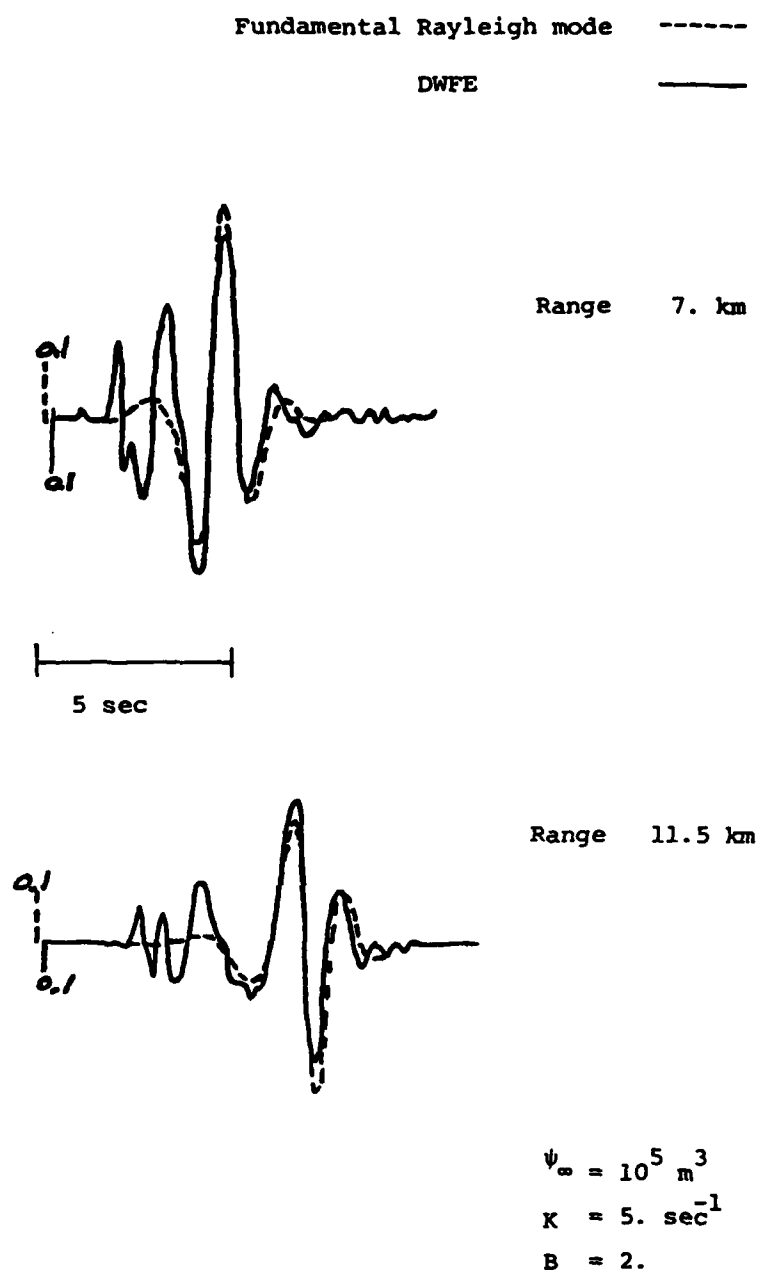
Figure 6. Comparison of DWFE calculations with fundamental
Rayleigh mode.
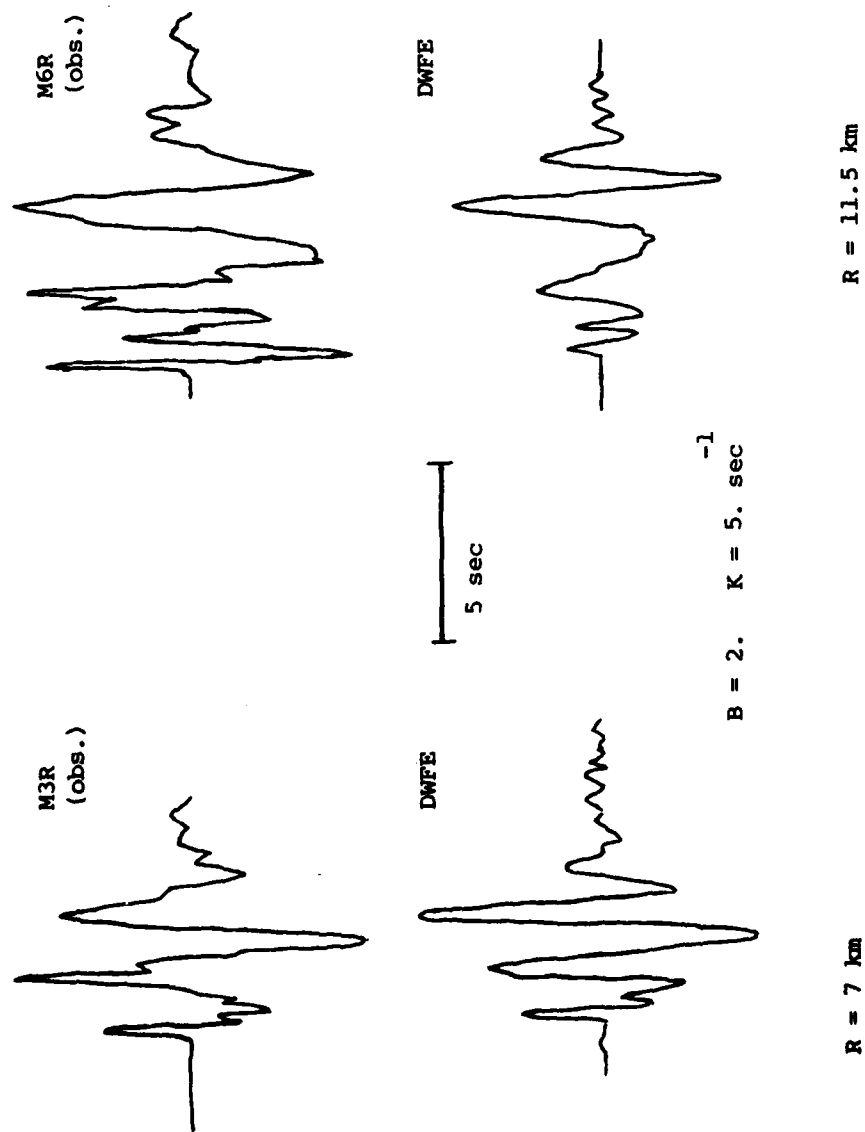
Figure 7. Comparison of DWFE calculations and radial velocities for stations 3 and 6.

Range 7. km

1 sec
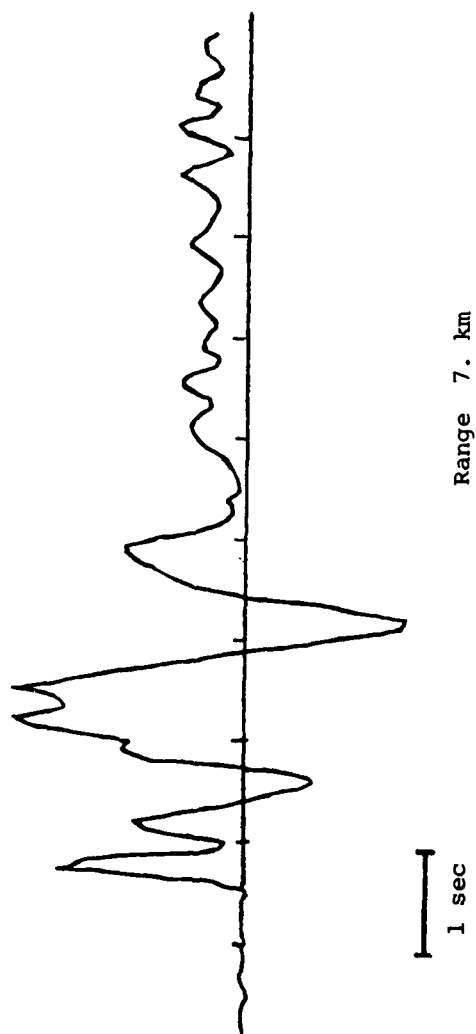
Figure 8. Radial ground displacement for step explosion moment – DWFE.

23
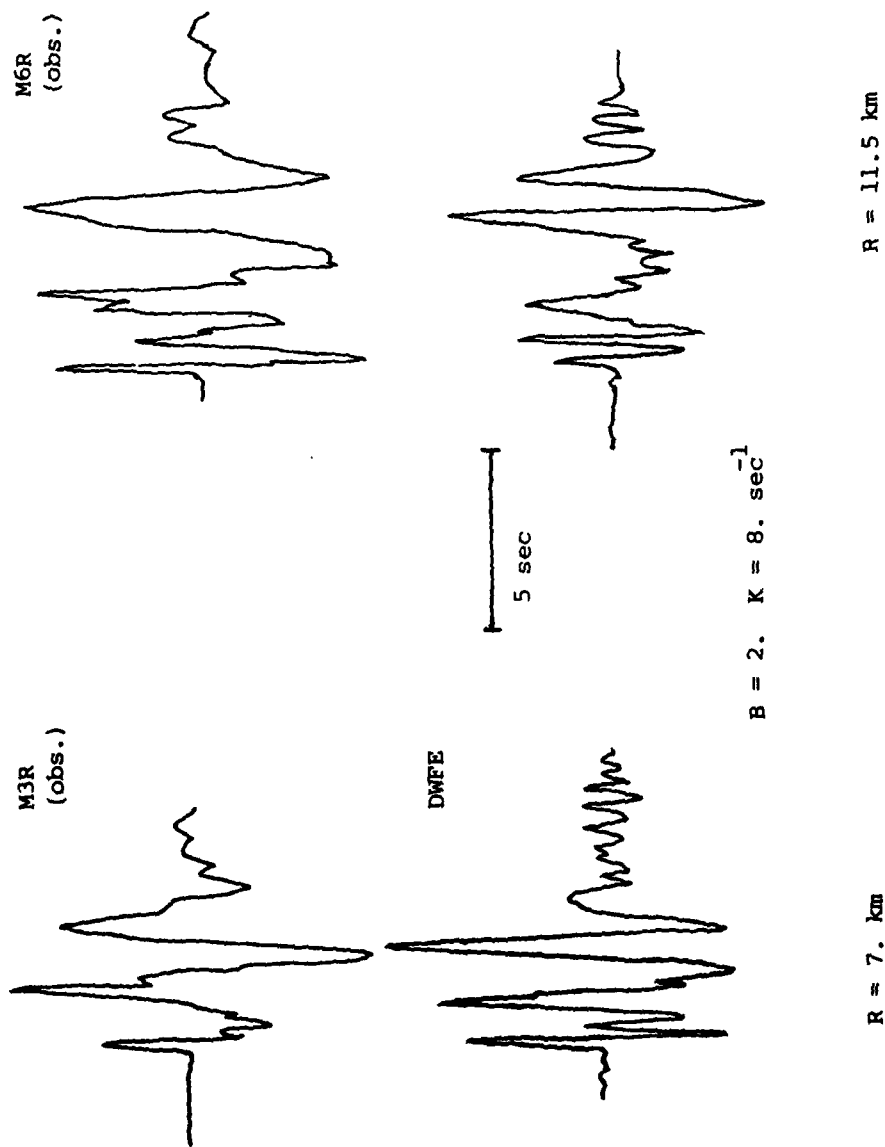
Figure 9. DWFE synthetics for two radial components using a more step-like RDP.
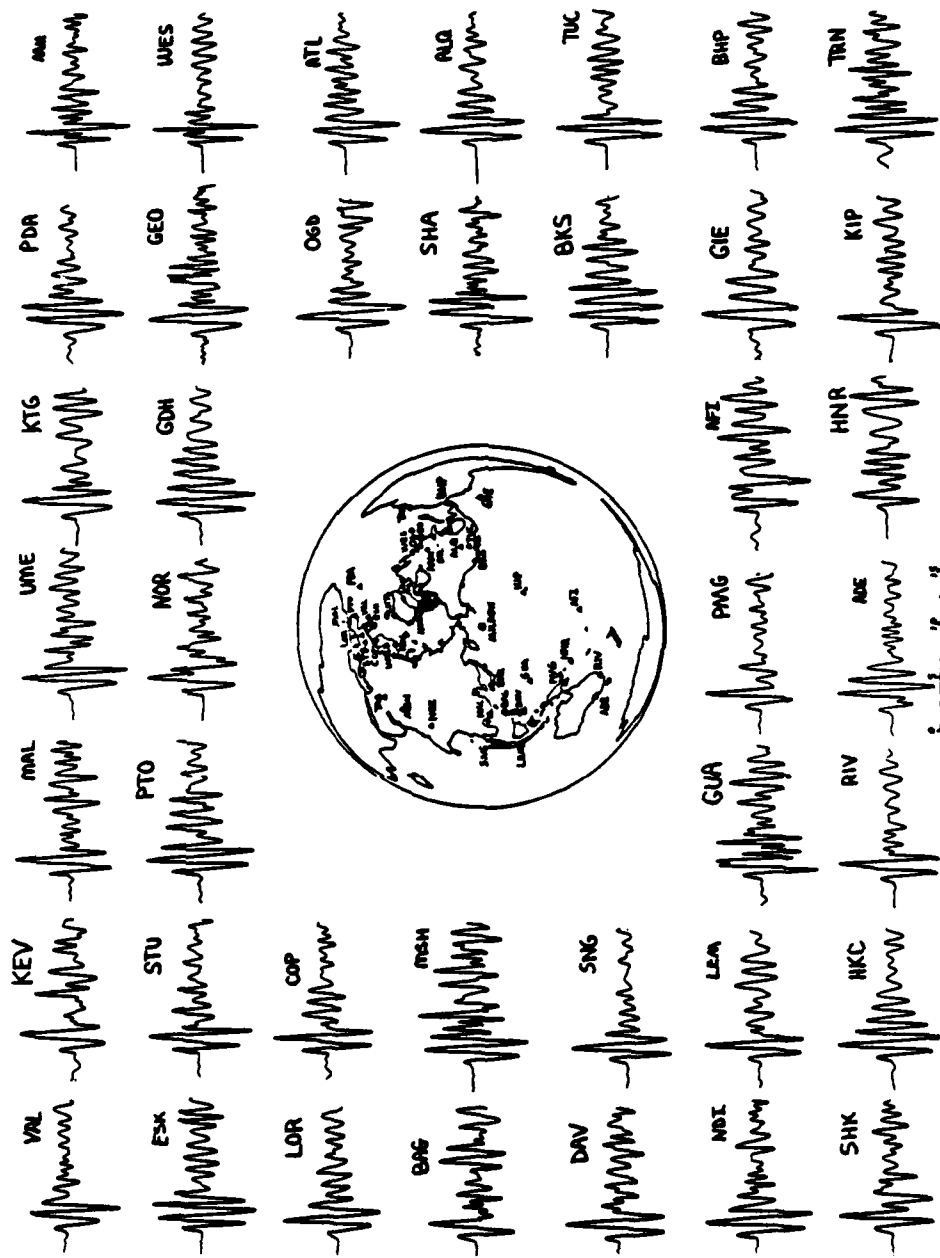
Figure 10. WWSSN recordings of P waveforms for Milrow.

25
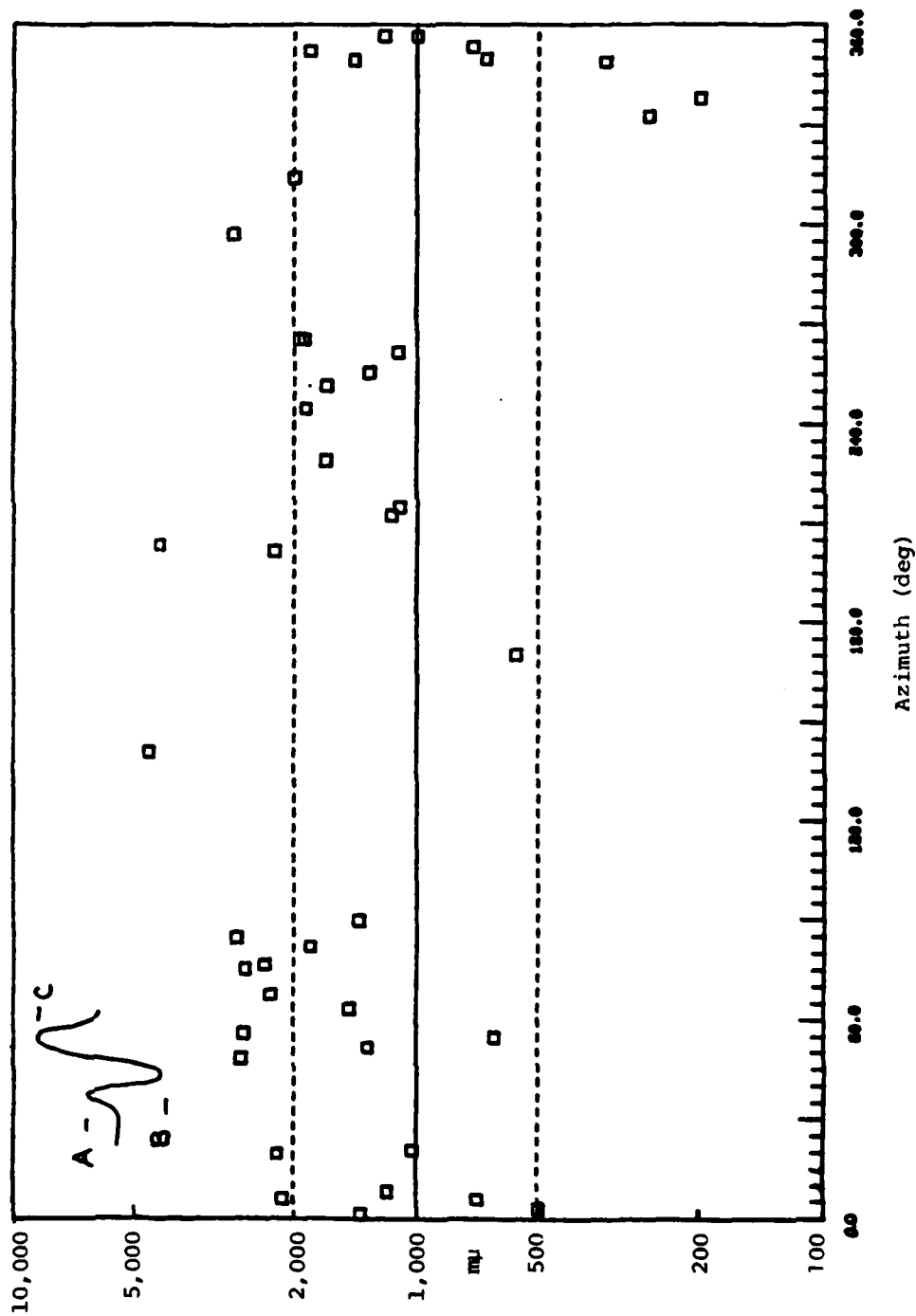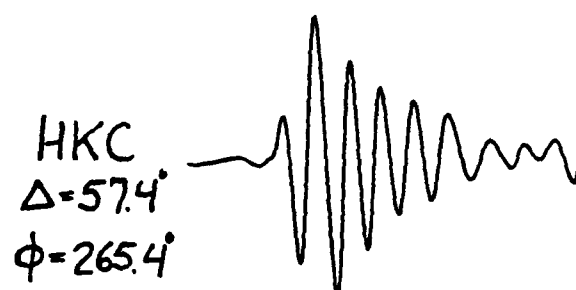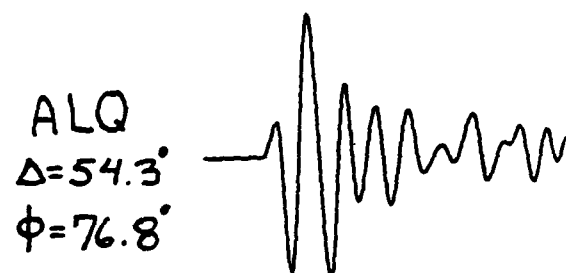
Figure 11. AB amplitudes for Milrow corrected to 30°.
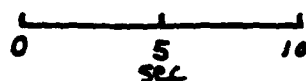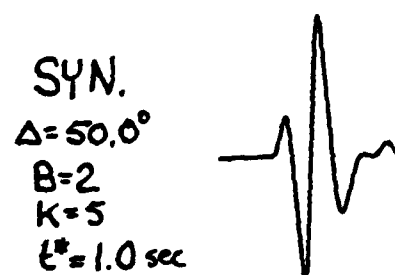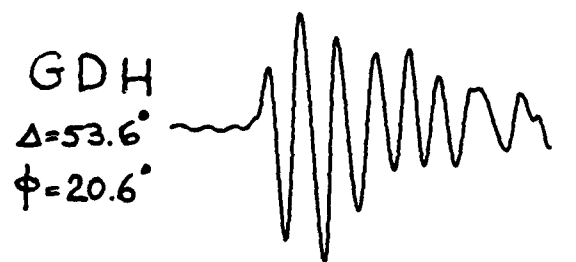
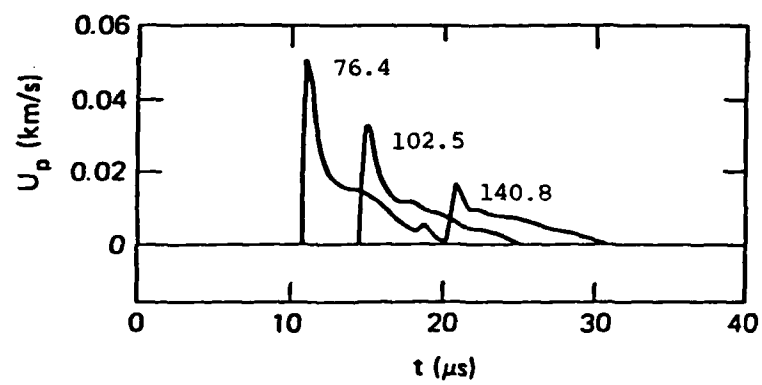Figure 12. Synthetic at 50° compared to data at nearly 50°.

Figure 13. Radial velocity data at radii 76.4,
102.5 and 140.8 mm for Blair dolomite, charge radius
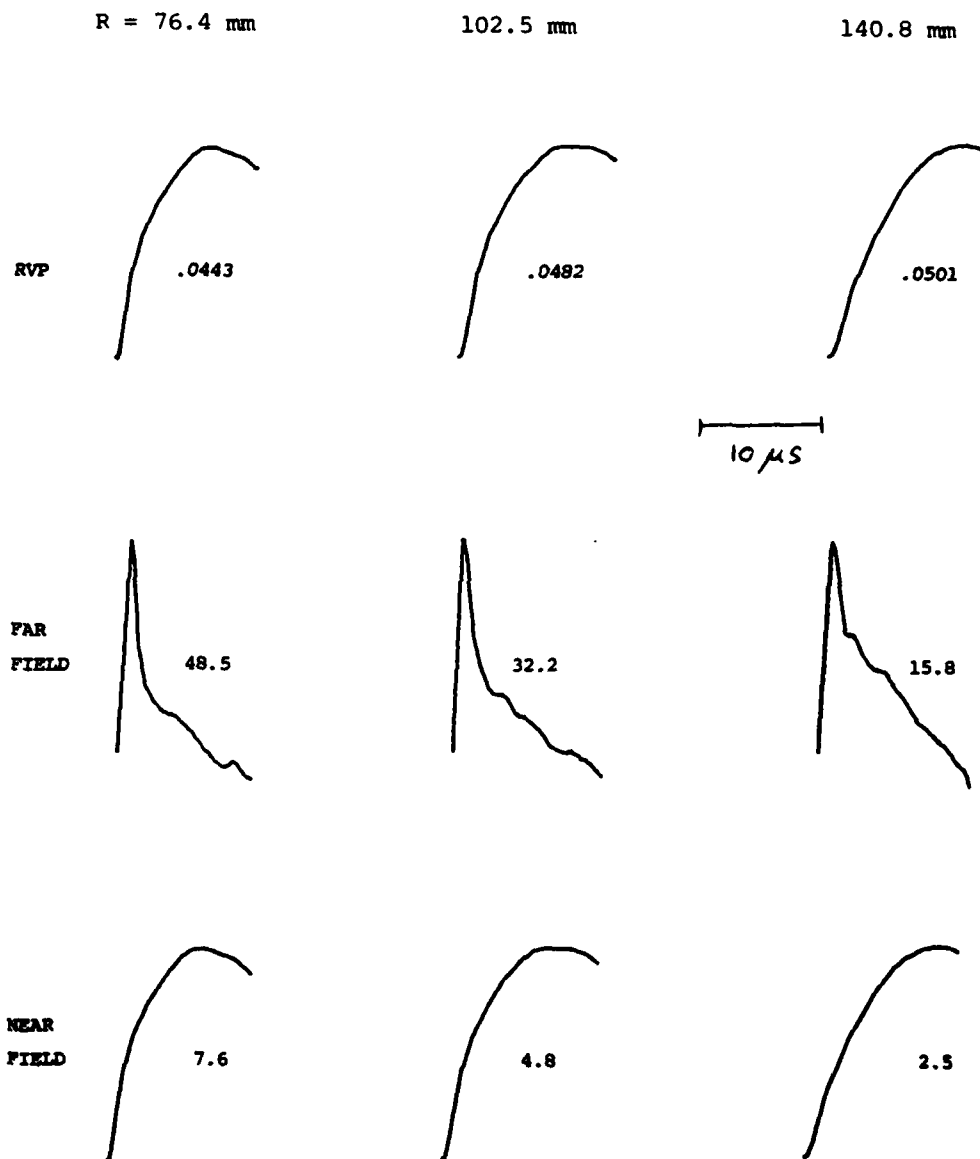9.5 mm. Modified after Larson (1981), Figure 3a.

R = 76.4 mm   102.5 mm   140.8 mm

RVP   .0443   .0482   .0501

$\vdash\!\!-\!\!-\!\!-\!\!\dashv$
10 µs

FAR
FIELD   48.5   32.2   15.8

NEAR
FIELD   7.6   4.8   2.5

Figure 14. RVP, Far Field velocity and Near Field velocity for
Blair dolomite at three ranges. Maximum amplitude is noted by
each trace. Units are m^3/s and m/s.

Data Radius

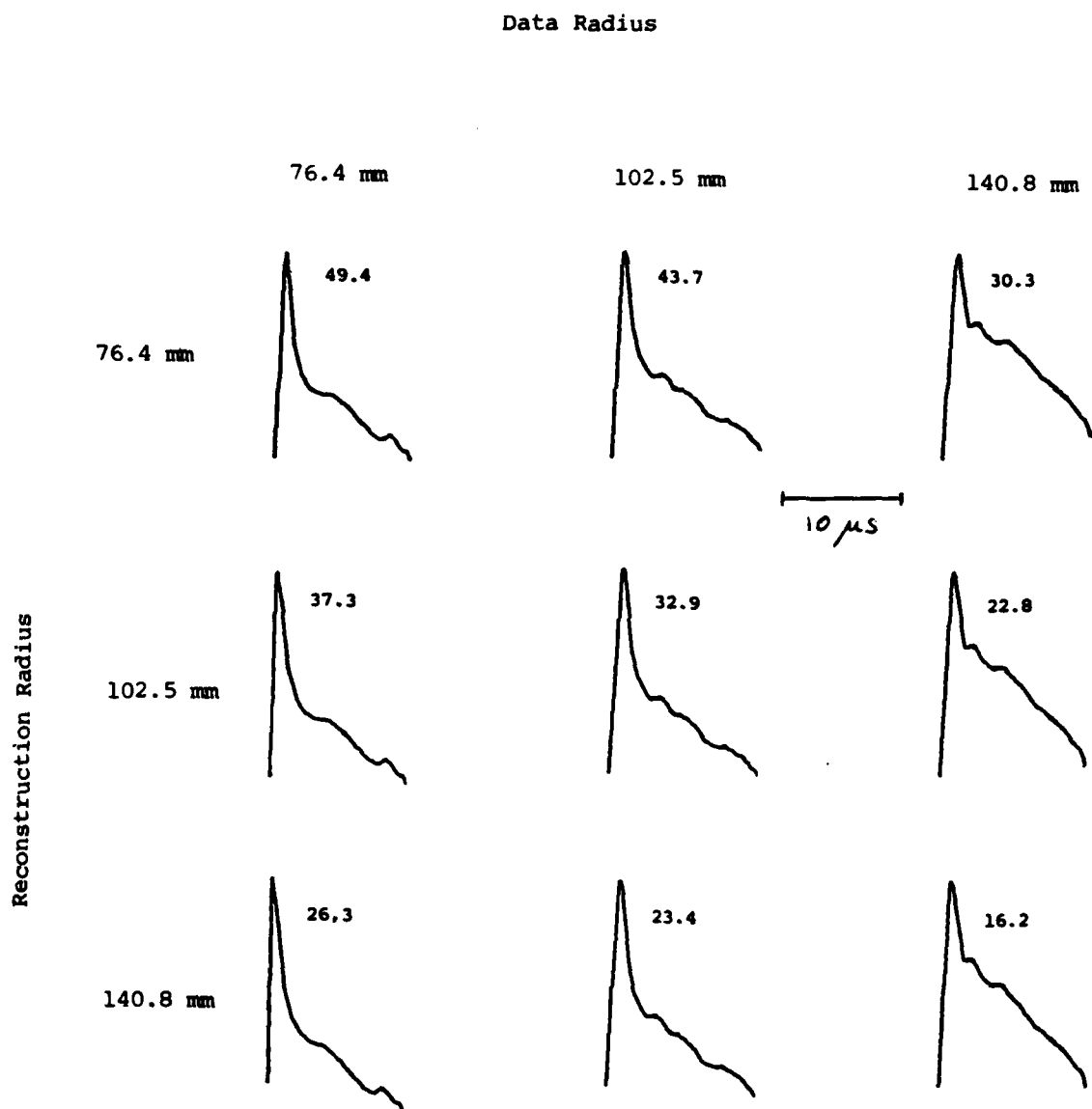76.4 mm   102.5 mm   140.8 mm

Figure 15. Velocities reconstituted from RVP's. Columns are measurement location. Rows are reconstitution locations. Maximum amplitudes are indicated (m/sec). Under ideally elastic conditions, the rows would consist of identical traces.

30